Integrated Segmentation and Nonrigid Registration for Application in Prostate Image-Guided Radiotherapy

Chao Lu[1,⋆], Sudhakar Chelikani[2], Zhe Chen[2], Xenophon Papademetris[2], Lawrence H. Staib[1,2], and James S. Duncan[1,2]

[1] Department of Electrical Engineering
[2] Department of Diagnostic Radiology
Yale University, New Haven, CT, USA
chao.lu@yale.edu

Abstract. Many current image-guided radiotherapy (IGRT) systems incorporate an in-room cone-beam CT (CBCT) with a radiotherapy linear accelerator for treatment day imaging. Segmentation of key anatomical structures (prostate and surrounding organs) in 3DCBCT images as well as registration between planning and treatment images are essential for determining many important treatment parameters. Due to the image quality of CBCT, previous work typically uses manual segmentation of the soft tissues and then registers the images based on the manual segmentation. In this paper, an integrated automatic segmentation/constrained nonrigid registration is presented, which can achieve these two aims simultaneously. This method is tested using 24 sets of real patient data. Quantitative results show that the automatic segmentation produces results that have an accuracy comparable to manual segmentation, while the registration part significantly outperforms both rigid and non-rigid registration. Clinical application also shows promising results.

1 Introduction

Prostate cancer is the most commonly diagnosed cancer among men in the United States. For the majority, external beam radiotherapy (EBRT) is one of the primary treatment modalities for prostate cancer [1].

Recent advances in EBRT have led to three-dimensional conformal radiotherapy (3DCRT) and intensity modulated radiotherapy(IMRT). Prostate 3DCRT requires a precise delineation of the target volume and the adjacent critical organs in order to deliver an optimal dose to the prostate with minimal side effect on nearby normal tissues. Many current image-guided radiotherapy (IGRT) systems integrate an in-room cone-beam CT (CBCT) with a radiotherapy linear accelerator for treatment day imaging. With both imaging and radiotherapy available on the same platform, daily CBCTs can now be acquired and used for patient positioning.

⋆ This work is supported by NIH/NIBIB Grant R01EB002164.

T. Jiang et al. (Eds.): MICCAI 2010, Part I, LNCS 6361, pp. 53–60, 2010.

However, when higher doses are to be delivered, precise and accurate targeting is essential because of unpredictable inter- and intra-fractional organ motions over the process of the daily treatments that often last more than one month. Therefore, a non-rigid registration problem must be solved in order to map the planning setup information in the initial 3DCT data into each treatment day 3DCBCT image. Meanwhile, we must acurately segment the prostate, bladder and rectum from the 3DCBCT images. Due to the quality of CBCT images, these issues can be very tough. Greene *et al.* [2] carried out this by manual segmentation and then involved nonrigid registration. Some initial work has been performed in simultaneously integrating registration and segmentation. Chelikani *et al.* [3] integrated rigid 2D portal to 3D CT registration and pixel classification in an entropy-based formulation. Yezzi *et al.* [4] integrated segmentation using level sets with rigid and affine registration. Chen *et al.* [5] implemented a nonrigid transformation and a hidden Markov random field to improve the segmentation performance.

In this paper, we present an integrated automatic segmentation and softly constrained nonrigid registration algorithm. Our model is based on a *maximum a posteriori*(MAP) framework while the automatic segmentation is performed using level set deformable model with shape prior information, as proposed in [6], and the constrained nonrigid registration part is based on a multi-resolution cubic B-spline Free Form Deformation (FFD) transformation. These two issues are intimately related: by combining segmentation and registration, we can recover the treatment fraction image regions that correspond to the organs of interest (prostate, bladder, rectum) by incorporating transformed planning day organs to guide and constrain the segmentation process; and conversely, accurate knowledge of important soft tissue structures will enable us achieve more precise nonrigid registration which allows the clinician to set tighter planning margins around the target volume in the treatment plan. Escalated dosages can then be administered while maintaining or lowering normal tissue irradiation.

2 Method

The integrated segmentation/registration algorithm was developed using Bayesian analysis to calculate the most likely segmentation in treatment day fractions S_d and the mapping field between the planning day data and treatment day data T_{0d}. This algorithm requires: (1) a planning day 3DCT image I_0, (2) a treatment day 3DCBCT image I_d, and (3) the segmented planning day organs S_0.

2.1 MAP Framework

A probabilistic model can be used to realize image segmentation combining prior information and image information, simultaneously, it can also realize

nonrigid registration by incorporating both intensity matching and segmented organ matching constraint. Thus we estimate

$$\widehat{S_d}, \widehat{T_{0d}} = \arg \max_{S_d, T_{0d}} [p(S_d, T_{0d} | I_0, I_d, S_0)] \tag{1}$$

This multiparameter MAP estimation problem in general is difficult to solve, however, we reformulate this problem such that it can be solved in two basic iterative computational stages using an iterative conditional mode (ICM) strategy. With k indexing each iterative step, we have:

$$\widehat{S_d^k} = \arg \max_{S_d^k} [p(S_d^k | T_{0d}^k(S_0), I_d)] \tag{2}$$

$$\widehat{T_{0d}^{k+1}} = \arg \max_{T_{0d}^{k+1}} [p(T_{0d}^{k+1} | S_d^k, S_0, I_d, I_0)] \tag{3}$$

These two equations represent the key problems we are addressing: i.) in equation (2) the estimation of the segmentation of the important day d structures (S_d^k) and ii.) in equation (3), the estimation at the next iterative step of the mapping T_{0d}^{k+1} between the day 0 and day d spaces.

2.2 Segmentation Module

We first apply Bayes rule to equation (2) to get:

$$\widehat{S_d^k} = \arg \max_{S_d^k} [p(S_d^k | T_{0d}^k(S_0), I_d)] = \arg \max_{S_d^k} [p(I_d | S_d^k) p(T_{0d}^k(S_0) | S_d^k) p(S_d)] \tag{4}$$

Here we assume that the priors are stationary over the iterations, so we can drop the k index for that term only, i.e. $p(S_d^k) = p(S_d)$. To build a model for the shape prior, we choose level sets as the representation of the objects. Consider a training set of n aligned images. Each object in the training set is embedded as the zero level set of a higher dimensional level set Ψ. The mean and variance of the boundary of each object can be computed using Principal Component Analysis (PCA). The mean level set,$\bar{\Psi}$, is subtracted from each Ψ to create the deviation. Each such deviation is placed as a column vector in a $N^3 \times n$-dimensional matrix Q where N^3 is the number of samples of each level set function. Using Singular Value Decomposition (SVD), $Q = U \Sigma V^T$. U is a matrix whose column vectors represent the set of orthogonal modes of shape variation and Σ is a diagonal matrix of corresponding singular values. An estimate of the object shape Ψ_i can be represented by k principal components and a k-dimensional vector of coefficients α_i: $\widetilde{\Psi}_i = U_k \alpha_i + \bar{\Psi}$. Under the assumption of a Gaussian distribution of object represented by α_i, we can compute the probability of a certain shape:

$$p(S_d) = p(\alpha_i) = \frac{1}{\sqrt{(2\pi)^k \, |\Sigma_k|}} exp \left[-\frac{1}{2} \alpha_i^T \Sigma_k^{-1} \alpha_i \right] \tag{5}$$

Then we impose a key assumption: the segmentation likelihood is separable into two independent data-related likelihoods, requiring that the estimate of the

structure at day d be close to: i.) the same structure segmented at day 0, but mapped to a new estimated position by the current iterative mapping estimate T_{od}^k and ii.) the intensity-based feature information derived from the day d image.

In equation (4), $p(T_{0d}^k(S_0)|S_d^k)$ constrains the segmentation in day d to be adherent to the transformed day 0 organs by current mapping T_{od}^k. Thus, the probability density of day 0 segmentation likelihood term can be modeled as:

$$p(T_{0d}^k(S_0)|S_d^k) = \frac{1}{Z} \prod_{(x,y,z)} exp\left[-(\Psi_{T_{0d}^k(S_0)} - \Psi_{S_d^k})^2\right] \tag{6}$$

where Z is a normalizing constant. Assuming gray level homogeneity within each object, we use the imaging model defined by Chan [7], where c_1 and σ_1 are the average and standard deviation of I_d inside S_d^k, c_2 and σ_2 outside.

$$p(I_d|S_d^k) = \prod_{inside(S_d^k)} exp[-(I_d(x,y,z)-c_1)^2/2\sigma_1^2] \cdot \prod_{outside(S_d^k)} exp[-(I_d(x,y,z)-c_2)^2/2\sigma_2^2] \tag{7}$$

Notice that the MAP estimation of the objects in equation (4), $\widehat{S_d^k}$, is also the minimizer of the energy function E_{seg} shown below. This minimization problem can be formulated and solved using the level set surface evolving method.

$$\begin{aligned} E_{seg} &= -lnp(S_d^k|T_{0d}^k(S_0), I_d) = -ln[p(I_d|S_d^k) \cdot p(T_{0d}^k(S_0)|S_d^k) \cdot p(S_d^k)] \\ &\propto \lambda_1 \int_{inside(S_d^k)} |I_d(x,y,z) - c_1|^2 \, dxdydz + \lambda_2 \int_{outside(S_d^k)} |I_d(x,y,z) - c_2|^2 \, dxdydz \\ &+ \gamma \int_{(x,y,z)} \left|\Psi_{T_{0d}^k(S_0)} - \Psi_{S_d^k}\right|^2 dxdydz + \omega_i \alpha_i^T \Sigma_k^{-1} \alpha_i \end{aligned} \tag{8}$$

2.3 Registration Module

The goal here is to register the planning day data to the treatment day data and carry the planning information forward, as well as to carry forward segmentation constraints. To do this, the second stage of the ICM strategy described above in equation (3) can be further developed using Bayes rule:

$$\begin{aligned} \widehat{T_{0d}^{k+1}} &= \arg\max_{T_{0d}^{k+1}} [p(T_{0d}^{k+1}|S_d^k, S_0, I_d, I_0)] \\ &= \arg\max_{T_{0d}^{k+1}} \left[\ln p(S_d^k, S_0|T_{0d}^{k+1}) + \ln p(I_d, I_0|T_{0d}^{k+1}) + \ln p(T_{0d})\right] \end{aligned} \tag{9}$$

The first two terms on the right hand side represent conditional likelihoods related to first registering the three segmented soft tissue structures at days 0 and d, and second registering the intensities of the images. The third term represents prior assumptions on the overall nonrigid mapping, which is captured with smoothness models and is assumed to be stationary over the iterations.

As discussed in the segmentation section, each object is represented by the zero level set of a higher dimensional level set Ψ. Assuming the objects vary

during the treatment process according to a Gaussian distribution, and given that the different organs can be registered respectively, we further simplifies the organ matching term as

$$\begin{aligned}\ln p(S_d^k, S_0|T_{0d}^{k+1}) &= \sum_{obj=1}^{3} \ln p(S_{d-obj}^k, S_{0-obj}|T_{0d}^{k+1}) \\ &= \sum_{obj=1}^{3} \int_{(x,y,z)} \ln \frac{1}{\sqrt{2\pi}\sigma_{obj}} \exp\left[\frac{-(\Psi_{T_{0d}^{k+1}(S_{0-obj})} - \Psi_{S_{d-obj}^k})^2}{2\sigma_{obj}^2}\right] dxdydz \\ &= \sum_{obj=1}^{3} -\omega_{obj} \int_{(x,y,z)} \left[\Psi_{T_{0d}^{k+1}(S_{0-obj})} - \Psi_{S_{d-obj}^k}\right]^2 dxdydz\end{aligned} \tag{10}$$

When minimized, the organ matching term ensures the transformed day 0 organs and the segmented day d organs align over the regions.

The intensities of CT and CBCT differ by a linear transformation and Gaussian noise due to X-ray scatter during CBCT acquisition. In this paper, normalized cross correlation (NCC), which has successfully been tested in prostate IGRT[2], is used to address such intensity matching objective.

$$C_{NCC} = -\ln p(I_d, I_0|T_{0d}^{k+1}) = -\frac{1}{N}\int_{x,y,z} \frac{\left[T_{0d}^{k+1}(I_0(x,y,z)) - \bar{I}_0\right]\left[I_d(x,y,z)) - \bar{I}_d\right]}{\sigma_{T_{0d}^{k+1}(I_0)}\sigma_{I_d}} dxdydz \tag{11}$$

where $\bar{I}_0$ and $\bar{I}_d$ are the mean intensities, σ represents the standard deviation.

To ensure a transformation is smooth, a penalty term is also introduced.

$$C_{smooth} = -\ln p(T_{0d}) = \frac{1}{V}\int_{x,y,z} [(\frac{\partial^2 T_{0d}}{\partial x^2})^2 + (\frac{\partial^2 T_{0d}}{\partial y^2})^2 + (\frac{\partial^2 T_{0d}}{\partial z^2})^2] dxdydz \tag{12}$$

where V denotes the volume of the image domain. The regularization term penalizes only nonaffine transformations. In addition, we constrain each control point of the tensor B-Spline FFD to move within a local sphere of radius $r < R$ where $R \approx 0.4033$ of the control point spacing. This condition guarantees T_{0d} to be locally injective[2].

Therefore, we introduce the registration energy function that can be minimized using a conjugate gradient optimizer,

$$\begin{aligned}E_{reg} &= -\ln p(T_{0d}^{(k+1)}|S_d^k, S_0, I_d, I_0) \\ &= -\ln p(S_d^k, S_0|T_{0d}^{(k+1)}) - \ln p(I_d, I_0|T_{0d}^{(k+1)}) - \ln p(T_{0d}) \\ &= \sum_{obj=1}^{3} \omega_{obj} \int_{x,y,z} \left[\Psi_{T_{0d}^{k+1}(S_0)} - \Psi_{S_d^k}\right]^2 dxdydz + C_{NCC} + \beta C_{smooth}\end{aligned} \tag{13}$$

Equations (8) and (13) run alternatively until convergence. Thereafter, the soft tissue segmentation as well as the nonrigid registration benefit from each other and can be estimated simultaneously.

3 Results

We tested our iterative conditional model (ICM) on 24 sets of real patient data acquired from three different patients. Each of the patient had eight treatment 3D CBCT images, and had an associated planning day 3DCT image and 3DCRT treatment plan. The planning day prostate, rectum, and bladder were hand segmented by a qualified clinician. The experiment results are presented below.

3.1 Segmentation and Registration Results

In Fig.1(a), we show the sagittal view of the segmentation using only image gray level information from treatment day CBCT data, by which the surfaces cannot lock onto the shapes of the objects, since these structures have very poorly defined boundaries. Fig.1(b) shows the results using gray level information with the shape prior. The results are better, but the boundaries of the organs overlap a lot where the structures are connected. In Fig.1(c), we show results of using our ICM model. The three structures can be clearly segmented. The surfaces are able to converge on the desired boundaries even though some parts of the boundaries are too blurred to be detected by gray level information, and there is no overlap of the boundaries due to the use of constraints from transformed planning day organs. Fig.1(d) shows the clinician's manual segmentation for comparison.

To validate the segmentation results, we tested our model on 24 treatment day images and then compared with the manual results (used as ground truth) using three metrics: mean absolute distance(MAD), Hausdorff distance (HD), and the percentage of correctly segmented voxels (PTP). While MAD represents the global disagreement between two contours, HD compares their local similarities. Quantitative validation in Table 1 showed remarkable and consistent agreement between the proposed method and manual segmentation by expert.

The registration performance of the proposed ICM algorithm was also evaluated. For comparison, a conventional non-rigid registration (NRR) using only intensity matching and rigid registration (RR) were performed on the same 24 sets of real patient data. Organ overlaps between the ground truth in day d and the transformed organs from day 0, as well as the mutual information between CBCT and transformed CT images were used as metrics to assess the quality of the registration (Table 2). The overlap increase for each object and the increase of mutual information after 10 iterations are presented in Fig.2.

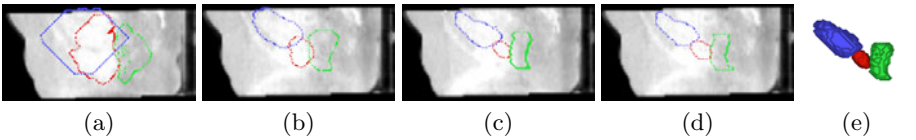

Fig. 1. Segmentation performance. Red:prostate, Blue:bladder, Green:rectum. (a)Using gray level information; (b)With Shape prior; (c)Proposed ICM algorithm; (d)Manual segmentation; (e)Segmented 3D Surfaces using the proposed method.

Table 1. Evaluation of the Segmentation Module

	Method	MAD(mm)	HD(mm)	PTV(%)
Prostate	shape prior	7.84 ± 2.69	9.13 ± 3.18	62.04 ± 4.73
	ICM model	1.92 ± 0.45	2.56 ± 0.75	96.15 ± 2.70
Bladder	shape prior	10.21 ± 5.39	11.28 ± 5.84	63.79 ± 3.72
	ICM model	2.84 ± 0.67	4.23 ± 1.19	94.69 ± 3.59
Rectum	shape prior	9.55 ± 4.76	10.97 ± 5.53	56.66 ± 10.86
	ICM model	2.59 ± 0.58	3.46 ± 1.05	92.72 ± 2.83

Table 2. Evaluation of the Registration Module

	RR	NRR	ICM
Prostate Overlap(%)	45.32 ± 2.45	77.58 ± 4.14	92.65 ± 1.82
Bladder Overlap(%)	61.85 ± 3.73	73.23 ± 8.28	94.79 ± 2.44
Rectum Overlap(%)	41.96 ± 4.16	64.27 ± 6.32	90.13 ± 2.83
Mutual Information	0.92 ± 0.09	1.26 ± 0.18	1.38 ± 0.25

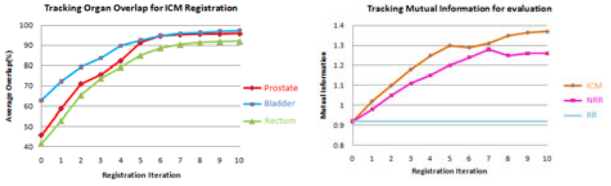

(a) (b)

Fig. 2. Registration performance. (a)Average object overlap results at each iteration using the proposed algorithm; (b)Comparison of ICM results to NRR and RR using mutual information at each iteration;

The RR performed the poorest out of all the registrations algorithms, generating an identity transform for all sets of patient data, while the proposed ICM method significantly outperformed the NRR at aligning segmented organs. All results presented here were averaged over the 24 sets of real patient data.

3.2 Treatment Plan Results: Cumulative Dose Distribution

Due to set-up errors and organ motions, treatment plan results varied from day to day. For this reason, it is essential to characterize the dose delivered to each region of interest. The nonrigid transformation achieved using our model was used to warp a fixed dose plan at each treatment day and compute the dose delivered to each voxel of tissue by properly accumulating the warped dose over all treatment fractions. Fig.3 (left) shows a 2D slice through 3D cumulative dose distribution when dose plans(12mm margin) were mapped and summed across 8 weekly treatment fractions from a single patient. Though it is apparent that the prostate is receiving nearly 90% of the dose, the bladder and the rectum are also receiving substantial amounts. Since our method could achieve a more accurate segmentation and registration, it enables the clinician to set a tighter margin (4mm) prescribed around the Clinical Target Volume (CTV), to ensure accurate delivery of the planned dose to the prostate and to minimize the dose received by the rectum and bladder, as shown in Fig.3 (right).

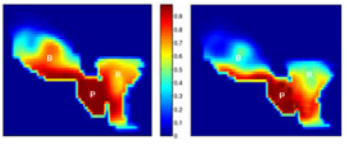

Fig. 3. Cumulative dose distributions for plans with 12mm(left) and 4mm(right) margin

4 Conclusion

In this paper, we have presented a novel integrated iterative conditional model that could simultaneously achieve automatic segmentation and constrained nonrigid registration. Experiments on 24 sets of real patient data showed that automatic segmentation using the ICM produced results that had an accuracy comparable to that obtained by manual segmentation. For each patient data tested, the proposed method proved to be highly robust and significantly improved the overlap for each soft tissue organ and outperformed the results achieved from the RR and NRR. Updating treatment plans showed promising superiority of the novel method in maintaining radiation dosage to the prostate and lowering radiation dosage to the rectum and bladder. Therefore, the proposed algorithm appears suitable for clinical application in image-guided radiotherapy analysis. Future work would focus on pelvic anatomy incorporating shape prediction. We can potentially adjust the plan to better conform to the dose already delivered and match the predicted variability in the pelvic anatomy for future fractions.

References

1. Potosky, A.L., Legler, J., Albertsen, P.C., Stanford, J.L., Gilliland, F.D., Hamilton, A.S., Stephenson, R.A., Harlan, L.C.: Health outcomes after prostatectomy or radiotherap for prostate cancer: Results from the prostate cancer outcomes study. J. Nat. Cancer Inst. 92, 1582–1592 (2000)
2. Greene, W.H., Chelikani, S., Purushothaman, K., Chen, Z., Knisely, J.P.S., Staib, L.H., Papademetris, X., Duncan, J.S.: A Constrained Non-rigid Registration Algorithm for Use in Prostate Image-Guided Radiotherapy. In: Metaxas, D., Axel, L., Fichtinger, G., Székely, G. (eds.) MICCAI 2008, Part I. LNCS, vol. 5241, pp. 780–788. Springer, Heidelberg (2008)
3. Chelikani, S., Purushothaman, K., Knisely, J., Chen, Z., Nath, R., Bansal, R., Duncan, J.S.: A gradient feature weighted minima algorithm for registration of multiple portal images to 3DCT volumes in prostate radiotherapy. Int. J. Radiation Oncology Biol. Phys. 65, 535–547 (2006)
4. Yezzi, A., Zollei, L., Kapur, T.: A variational framework for integrating segmentation and registration through active contours. Medical Image Analysis 7, 171–185 (2000)
5. Chen, X., Brady, M., Rueckert, D.: Simultaneous segmentation and registration for medical image. In: Barillot, C., Haynor, D.R., Hellier, P. (eds.) MICCAI 2004. LNCS, vol. 3216, pp. 663–670. Springer, Heidelberg (2004)
6. Leventon, M.E., Faugeras, O., Grimson, W.E.L., Wells III, W.M.: Level Set Based Segmentation with Intensity and Curvature Priors. In: Proc. MMBIA 2000, pp. 4–11 (2000)
7. Chan, T., Vese, L.: Active Contours Without Edges. IEEE Transactions on Image Processing 10(2), 266–277 (2001)